Role of phase matching in pulsed second-harmonic generation: Walk-off and phase-locked twin pulses in negative-index media

Vito Roppo, Marco Centini, Concita Sibilia, and Mario Bertolotti
Dipartimento di Energetica, University of Rome La Sapienza, Via Scarpa 16, Rome, Italy

Domenico de Ceglia, Michael Scalora, Neset Akozbek, and Mark J. Bloemer
Charles M. Bowden Research Facility, RDECOM, US Army Aviation and Missile Command, Redstone Arsenal, AL 35803, USA

Joseph W. Haus
Electro-Optics Program, University of Dayton, Dayton, Ohio 45469-0245, USA

Olga G. Kosareva and Valery P. Kandidov
International Laser Center, Physics Department, Moscow State University, Moscow 119992, Russia
(Received 1 May 2007; published 26 September 2007)

The present investigation is concerned with the study of pulsed second-harmonic generation under conditions of phase and group velocity mismatch, and generally low conversion efficiencies and pump intensities. In positive-index, nonmetallic materials, we generally find qualitative agreement with previous reports regarding the presence of a double-peaked second harmonic signal, which comprises a pulse that walks off and propagates at the nominal group velocity one expects at the second-harmonic frequency, and a second pulse that is "captured" and propagates under the pump pulse. We find that the origin of the double-peaked structure resides in a phase-locking mechanism that characterizes not only second-harmonic generation, but also $\chi^{(3)}$ processes and third-harmonic generation. The phase-locking mechanism that we describe occurs for arbitrarily small pump intensities, and so it is not a soliton effect, which usually relies on a threshold mechanism, although multicolor solitons display similar phase locking characteristics. Thus, in second harmonic generation a phase-matched component is *always* generated, even under conditions of material phase mismatch: This component is anomalous, because the material does not allow energy exchange between the pump and the second-harmonic beam. On the other hand, if the material is phase matched, phase locking and phase matching are indistinguishable, and the conversion process becomes efficient. We also report a similar phase-locking phenomenon in negative index materials. A spectral analysis of the pump and the generated signals reveals that the phase-locking phenomenon causes the forward moving, phase-locked second-harmonic pulse to experience the same negative index as the pump pulse, even though the index of refraction at the second-harmonic frequency is positive. Our analysis further shows that the reflected second-harmonic pulse generated at the interface and the forward-moving, phase-locked pulse appear to be part of the same pulse initially generated at the surface, part of which is immediately back-reflected, while the rest becomes trapped and dragged along by the pump pulse. These pulses thus constitute twin pulses generated at the interface, having the same negative wave vector, but propagating in opposite directions. Almost any break of the longitudinal symmetry, even an exceedingly small $\chi^{(2)}$ discontinuity, releases the trapped pulse which then propagates in the backward direction. These dynamics are indicative of very rich and intricate interactions that characterize ultrashort pulse propagation phenomena.

DOI: 10.1103/PhysRevA.76.033829 PACS number(s): 42.65.Ky, 42.25.Bs

INTRODUCTION

In 1961, with the generation of the second harmonic light using a beam from a ruby laser, Franken and his collaborators experimentally discovered second-harmonic generation (SHG), and so nonlinear optics was born [1]. Since then, SHG has become one of the most investigated and discussed nonlinear optical processes. Although the conversion efficiency reported at the time was quite small, the advent of phase-matching techniques [2,3] has made it possible to significantly boost SHG conversion rates. Countless, detailed theoretical studies of SHG have appeared since the seminal work by Armstrong *et al.* and Bloembergen *et al.* [4] in 1962. In fact, during the past four decades the study of SHG has mushroomed and evolved to the point that nonlinear $\chi^{(2)}$ processes are among the best understood nonlinear optical phenomena.

In more recent times, the study of second order processes has also been concerned with optical solitons, or localized electromagnetic pulses that can propagate long distances in nonlinear media without undergoing shape changes. Although solitons had originally been associated with cubic ($\chi^{(3)}$) nonlinear media, they are now also achieved in quadratic materials [5]. Because the primary reason to investigate SHG has consistently been the achievement of efficient frequency doubling, the emphasis has been on phase-matched interactions between the fundamental and the second-harmonic beams. Phase matching (PM) is a condition that essentially requires conservation of linear momentum that also facilitates energy flow from the pump to the second-

harmonic signal. However, it is a condition that does not generally occur naturally, and so the literature abounds with contributions that contain techniques and stratagems that attempt to circumvent a naturally occurring phase mismatch, in order to bring the interacting waves closer to ideal, phase-matched conditions [2,6–24].

The systematic study of nonlinear propagation phenomena at or very near phase-matching conditions has resulted in relatively few studies of SHG and related propagation phenomena in a phase mismatched (PMM) environment. In fact, from time to time workers have been confronted with situations where, in addition to the usual second-harmonic beam, a second component was observed. For example, the general solution for SHG from a boundary layer discussed in Refs. [4] is revealed as being composed of a reflected signal, and two forward propagating components, one displaying a k-vector that is a solution of the homogeneous wave equation (i.e., the expected wave vector at the second-harmonic frequency), and the other a k-vector that is the solution of the inhomogeneous wave equation, equal to twice the pump wave vector. Shapiro [25] in 1968 noted: "SHG spectra consisted of two parts: A part matched across the breadth of the laser fundamental…and a portion which remained fixed in frequency and coincided with the laser fundamental peak." The author thus appreciated that there were two SH components, but did not elaborate further on his findings.

In 1969, in a mathematical treatment Glenn [26] provided a general solution of the SH field that also showed two contributions, one arising as a surface term, traveling with the characteristic group velocity expected at the second harmonic frequency, and a second component that instead appeared to travel with the group velocity of the fundamental beam. These findings notwithstanding, workers' attention remained focused on efficient energy conversion schemes, via the implementation of quasi-phase-matching [27].

In 1987, Manassah *et al.* [28] theoretically showed that, in the weak conversion efficiency regime and in the presence of group velocity dispersion, the second-harmonic signal was characterized by a double-peaked structure. The effect was attributed to an interplay between $\chi^{(2)}$ and $\chi^{(3)}$ processes, and self- and cross-phase modulation that occurred during the interaction. Then, in 1990, Noordam *et al.* [29] reported that under conditions of a phase and group velocity mismatch, the second-harmonic signal indeed displayed two prominent features. In their words: "This letter is… the first report on the observation of double-peak shapes due to group velocity difference between the fundamental and the generated second harmonic."

In the years that followed, the phenomenon was again reported theoretically and experimentally. The high-intensity regime and the relatively high conversion efficiencies (up to 3.5%) however required that the interaction be placed in a context of competing second and third order processes [30]. Su *et al.* [31] introduced additional theoretical and experimental evidence that a purely second order process could lead to a double-peaked structure in the time domain profile of the second harmonic beam. The effect was attributed to induced group velocity dispersion (GVD), under conditions of negligible group velocity mismatch (GVM). As the pump and SH beam copropagate, they argued, the pump is able to impress its dispersive properties on the SH pulse, a process that may be viewed as induced effective dispersion.

Also recently, the double-peaked structure in the SH signal was discussed theoretically in the context of femtosecond pulse propagation in a birefringent nonlinear material, under phase-mismatched conditions [32]. In that study, the authors used a finite difference time domain (FDTD) method to solve Maxwell's equations in the presence of a material discontinuity that separated vacuum from a nonlinear medium. The result suggested that the SH signal splits into two components, one that travels at the pump's group velocity, and a second component that walks off, consistent with all previous predictions and observations of the phenomenon.

The present investigation is concerned with the study of pulsed SHG under conditions of phase and group velocity mismatch, and low conversion efficiencies and pump intensities, primarily in negative index materials. In positive index materials (PIMs, nonmetallic), we generally find qualitative agreement with all previous reports regarding the presence of a double-peaked second harmonic signal, and a SH pulse that propagates at the pump's group velocity. Instead, our results provide additional insight into the dynamical aspects and the interpretation of the phenomenon, in that we find that the origin of the double-peaked structure resides in a phase-locking mechanism that characterizes not only SHG, but also $\chi^{(3)}$ processes, for example, as shown in [33], where the phase-locking mechanism was first discussed in the context of intense field propagation and filamentation in the atmosphere. We find that the two peaks consist of a first peak that quickly phase-locks to the pump pulse and propagates under the pump envelope at the pump's group velocity, and a second component that propagates with the characteristic group velocity of the second-harmonic frequency, which we refer to as the normal component. At low intensities, the normal component propagates at the nominal group velocity given by linear material dispersion. Although we leave the details for future work, at relatively high intensities pulse separation can occur faster because the group velocity of the normal pulse also appears to be affected by the intensity of the incident field.

One point worthy of note is that the phase-locking mechanism that we describe occurs for arbitrarily small pump intensities. For this reason we believe it is not a soliton effect, which usually relies on a threshold mechanism [5,34–38]. In [38], for example, the effect is discussed at length within the context of continuous wave beams, diffraction, and associated spatial soliton formation, in both seeded and unseeded cases. The authors in fact coined the term "beam locking" to distinguish the phenomenon from other solitonlike effects that occur in $\chi^{(3)}$ media [38]. In our case, we find that once the normal component separates, the phase-locking is complete, the interaction between the waves ceases, and in the absence of pump focusing [33] the energy of the second harmonic pulse clamps.

In recent years, there has been a growing interest in artificially engineered metamaterials using subwavelength conducting resonant elements that exhibit unusual properties, including negative index of refraction [39]. Negative index metamaterials can be realized when both the electric permittivity and magnetic permeability are negative [40]. However,

known natural materials do not posses such a property. For example, at optical frequencies metals exhibit a negative permittivity, whereas the magnetic permeability is of order unity. The so-called split ring resonator (SRR) by Pendry [41] was shown to exhibit a negative magnetic permeability, thus paving the way for a negative index material. Negative index materials have been demonstrated in the microwave regime [42] where the fabrication of the resonant elements is relatively easy. There is now an effort to make negative index materials in the optical regime [43]. Encouraging developments in negative index materials have already been made in the near infrared [44]. Despite the fact that there have already been a number of studies done on nonlinear optics in negative index materials [45,49,57], many properties and effects remain to be explored.

The case of phase-matched, pulsed, relatively efficient SHG in negative index materials (NIMs) in the presence of realistic absorption has been studied previously [46]. In [46] it was noted that the forward-propagating pump pulse, which was tuned in a negative-index region, could be exactly phase-matched to the backward propagating SH signal, tuned in a region of positive index. We presently focus our attention on the dynamics of low pump intensity, phase-mismatched SHG. Although we realize that in the optical domain NIMs are still mostly mathematical constructs, at least in terms of a uniform, continuous medium, and that the precise origin of a $\chi^{(2)}$ will have to be determined, we nevertheless report a phase-locking phenomenon similar to what occurs in PIMs, but with much more interesting dynamical characteristics. For instance, unlike PIMs, backward SHG from an air-NIM interface can be as intense, relatively speaking, as the forward-generated SH signal. A spectral analysis reveals that the phase-locking phenomenon causes the forward moving SH signal to experience the same negative index as the pump pulse, even though the generated SH signal is tuned to a frequency where the index of refraction is positive. The subsequent introduction of a physical boundary with vanishingly small index discontinuity, e.g., the pulse is made to cross from a nonzero $\chi^{(2)}$ region into a region free of nonlinearities, is enough to cause the phase-locked SH pulse to be released, and to begin a journey in the backward direction. Our analysis thus shows that the backward-generated pulse and the forward-moving, phase-locked pulse appear to be part of the same pulse initially generated at the interface, part of which immediately exits the structure, while the rest becomes trapped and dragged along by the pump pulse. These pulses thus constitute twin pulses generated at the interface, having the same negative wave vector, but propagating in opposite directions, as revealed by a break in the translational symmetry of the material.

PROPAGATION METHOD

To model the dynamics of interacting short pulses we use the models detailed in Refs. [46,47], which include two independent approaches that yield identical results: A fast Fourier transform beam propagation method (FFT-BPM), and a finite difference time domain (FDTD) method. For details the reader may consult the references. However, for completeness, here we provide the most salient features of the FFT-BPM model that we use. We describe the fields as a superposition of harmonics, as follows:

$$\mathbf{E} = \hat{\mathbf{x}} \sum_{\ell=1}^{\infty} [E_{\ell\omega}(z,t) + \text{c.c.}] = \hat{\mathbf{x}} \sum_{\ell=1}^{\infty} [\mathcal{E}_{\ell\omega}(z,t) e^{i\ell(k_0 z - \omega_0 t)} + \text{c.c.}],$$

$$\mathbf{H} = \hat{\mathbf{y}} \sum_{\ell=1}^{\infty} [H_{\ell\omega}(z,t) + \text{c.c.}] = \hat{\mathbf{y}} \sum_{\ell=1}^{\infty} [\mathcal{H}_{\ell\omega}(z,t) e^{i\ell(k_0 z - \omega_0 t)} + \text{c.c.}], \tag{1}$$

where ℓ is a positive integer that denotes the ℓth harmonic, $k_0 = \omega_0/c$ is the free space wave vector, and ω_0 is the corresponding carrier pump frequency. In Eqs. (1), each harmonic is expressed as the product of a generic envelope function and oscillating factors that contain carrier wave vector and frequency. The pump pulse (or pulses) are assumed to be initially located in free space, and no assumptions are made about the envelope functions. The nonlinear polarization and magnetization that evolve inside the medium may also be described in a manner similar to Eqs. (1), each in terms of a generic envelope function and carrier wave vector and frequency. For second order nonlinear processes, we assume nonlinear polarization and magnetization of the type $P_{\text{NL}} = \chi_P^{(2)} E^2$, and $M_{\text{NL}} = \chi_M^{(2)} H^2$, where $\chi_P^{(2)}$ and $\chi_M^{(2)}$ are the respective electric and magnetic nonlinear coefficients, which in turn are also allowed to be arbitrary functions of position. The usual procedure then calls for the expansion of the nonlinear terms, and the collection of the various harmonics. For example, retaining terms up to the fourth harmonic frequency, the corresponding nonlinear polarization terms become

$$\mathcal{P}_\omega(z,t) = 2\chi_P^{(2)}(\mathcal{E}_\omega^* \mathcal{E}_{2\omega} + \mathcal{E}_{2\omega}^* \mathcal{E}_{3\omega} + \mathcal{E}_{3\omega}^* \mathcal{E}_{4\omega} + \cdots),$$

$$\mathcal{P}_{2\omega}(z,t) = \chi_P^{(2)}(\mathcal{E}_\omega^2 + 2\mathcal{E}_\omega^* \mathcal{E}_{3\omega} + 2\mathcal{E}_{2\omega}^* \mathcal{E}_{4\omega} + \cdots),$$

$$\mathcal{P}_{3\omega}(z,t) = 2\chi_P^{(2)}(\mathcal{E}_\omega \mathcal{E}_{2\omega} + \mathcal{E}_\omega^* \mathcal{E}_{4\omega} + \cdots),$$

$$\mathcal{P}_{4\omega}(z,t) = \chi_P^{(2)}(\mathcal{E}_{2\omega}^2 + 2\mathcal{E}_\omega \mathcal{E}_{3\omega} + \cdots). \tag{2}$$

The nonlinear magnetization terms have similar form. It follows that Maxwell's equations for the ℓth harmonic take the following form [46,47]:

$$\alpha_{\ell\tilde{\omega}} \frac{\partial \mathcal{E}_{\ell\tilde{\omega}}}{\partial \tau} \approx i\ell\beta(\varepsilon_{\ell\tilde{\omega},\xi} \mathcal{E}_{\ell\tilde{\omega}} - \mathcal{H}_{\ell\tilde{\omega}}) - \frac{\partial \mathcal{H}_{\ell\tilde{\omega}}}{\partial \xi} + 4\pi\left(i\ell\beta\mathcal{P}_{\ell\tilde{\omega}} - \frac{\partial \mathcal{P}_{\ell\tilde{\omega}}}{\partial \tau}\right),$$

$$\gamma_{\ell\tilde{\omega}} \frac{\partial \mathcal{H}_{\ell\tilde{\omega}}}{\partial \tau} \approx i\ell\beta(\mu_{\ell\tilde{\omega},\xi} \mathcal{H}_{\ell\tilde{\omega}} - \mathcal{E}_{\ell\tilde{\omega}}) - \frac{\partial \mathcal{E}_{\ell\tilde{\omega}}}{\partial \xi} + 4\pi\left(i\ell\beta\mathcal{M}_{\ell\tilde{\omega}} - \frac{\partial \mathcal{M}_{\ell\tilde{\omega}}}{\partial \tau}\right), \tag{3}$$

where $\alpha_{\ell\tilde{\omega}} = \partial[\tilde{\omega}\epsilon_{\ell\tilde{\omega}}(\xi)]/\partial\tilde{\omega}|_{\omega_0}$, $\gamma_{\ell\tilde{\omega}} = \partial[\tilde{\omega}\mu_{\ell\tilde{\omega}}(\xi)]/\partial\tilde{\omega}|_{\omega_0}$, and

the prime symbol denotes a derivative with respect to frequency; together with $\varepsilon_{\ell\tilde{\omega}}$ and $\mu_{\ell\tilde{\omega}}$, $\alpha_{\ell\tilde{\omega}}$ and $\gamma_{\ell\tilde{\omega}}$ are also complex functions of frequency and of the spatial coordinate. We have chosen $\lambda_0=1$ μm as the reference wavelength, and have adopted the following scaling: $\xi=z/\lambda_0$ is the scaled longitudinal coordinate (thus in microns); $\tau=ct/\lambda_0$ is the time in units of the optical cycle; $\beta=2\pi\tilde{\omega}$ is the scaled wave vector; $\tilde{\omega}=\omega/\omega_0$ is the scaled frequency, and $\omega_0=2\pi c/\lambda_0$, where c is the speed of light in vacuum.

The assumptions used to arrive at Eqs. (3) may be summarized as follows: (i) Second- and higher-order, linear material dispersion terms are neglected; (ii) third and higher harmonics are also neglected. As written, Eqs. (3) provide an accurate physical picture of the dynamics, including boundary conditions and all orders of reflections, even for pulses that are just a few wave cycles in duration [46,47].

To make sure that the approximations and assumptions discussed in the previous paragraphs are indeed valid, we also integrated Maxwell's equations using a finite difference, time domain algorithm similar to the one discussed in [48]. We then compared the solutions of Eqs. (3) to the solutions of the following set of equations [49]:

$$\frac{\partial E_x}{\partial t}=-\frac{1}{\varepsilon_0}\left[\frac{\partial H_y}{\partial z}+J_x\right]-\chi_e^{(2)}\frac{\partial E_x^2}{\partial t},\quad \frac{\partial J_x}{\partial t}+\Gamma_e J_x=\varepsilon_0\omega_e^2 E_x,$$

$$\frac{\partial H_y}{\partial t}=-\frac{1}{\mu_0}\left[\frac{\partial E_x}{\partial z}+K_y\right]-\chi_m^{(2)}\frac{\partial H_y^2}{\partial t},\quad \frac{\partial K_y}{\partial t}+\Gamma_m K_y=\mu_0\omega_m^2 H_y. \tag{4}$$

In Eq. (4), J_x and K_y are the electric and magnetic current densities, respectively, $\Gamma_{e,m}$ are the corresponding damping coefficients, and $\omega_{e,m}$ are the respective electric and magnetic plasma frequencies. The integration of Eqs. (3) and (4) were carried out for pulses whose durations varied from a few optical cycles up to several picoseconds, with indistinguishable results in all cases investigated. In addition to having more control over each term, Maxwell's equations (3) are written in a form that allows the use of the now classic fast Fourier transform, beam propagation method [50], appropriately modified to include all orders of reflections and feedback in the time domain [51]. We use a spectral method primarily because it is easily implemented as it involves multiplication of linear operators; it is unconditionally stable, with no known issues relating to phase or amplitude errors, and thus not prone to the generation of any numerical artifacts; and it can easily be extended to the multidimensional domain almost effortlessly [52,53].

SECOND HARMONIC GENERATION

The usual treatment of phase-matched SH generation in typical crystals follows this scheme: A plane wave at the fundamental frequency ω propagates with phase velocity $c/n(\omega)$ through a nonlinear $\chi^{(2)}$ medium, and a signal is thus generated at twice the temporal and spatial frequencies of the pump. Because typically one is concerned with maximizing the conversion efficiency of the process, it is desirable to keep the two waves as close as possible to the phase matching condition. This simply means that the indices of refraction at the fundamental and second harmonic frequencies are almost the same. In order to minimize pulse walkoff effects due to unequal group velocities, normally one also chooses the length of the nonlinear crystal to be much smaller than the spatial extension of the incident field. The typical situation may be illustrated with the following example: A nanosecond pulse, whose spatial extension is approximately 30 cm, may be incident on a millimeter- or centimeter-long crystal. However, if pulse length is comparable to the length of the structure or shorter, steps may also be taken to achieve so-called noncritical phase matching conditions, which occur when the group velocities of the FF and SH fields are also nearly matched, so that pulse walkoff effects are minimized. A number of strategies such as pulse prechirping and focusing may be adopted, and these and other techniques are summarized in [54], for example.

In the examples that follow, we will investigate SHG under conditions of normal material dispersion. The dispersion models that we adopt are as follows: The PIM is assumed to be composed of a standard dielectric material having a certain index mismatch between the FF and SH frequencies. The actual index mismatch depends on the material, but typical values may vary by as little as 5% or less for dielectrics, to 10–15 % or more for semiconductors, depending on how close to the electronic band edge one tunes the fields. The permittivity and the magnetic permeability of the NIM are described by a standard, lossy Drude model [55]:

$$\varepsilon(\tilde{\omega})=1-\frac{1}{\tilde{\omega}(\tilde{\omega}+i\tilde{\gamma}_e)},$$

$$\mu(\tilde{\omega})=1-\frac{\omega_{pm}/\omega_{pe}}{\tilde{\omega}(\tilde{\omega}+i\tilde{\gamma}_m)}, \tag{5}$$

where $\tilde{\omega}=\omega/\omega_{pe}$ is the normalized frequency, ω_{pe} and ω_{pm} are the respective electric and magnetic plasma frequencies, and $\tilde{\gamma}_e=\gamma_e/\omega_{pe}$ and $\tilde{\gamma}_m=\gamma_m/\omega_{pe}$ are the corresponding electric and magnetic loss terms normalized with respect to the electric plasma frequency. For simplicity, we assume that $\omega_{pe}=\omega_{pm}$ and $\gamma_e=\gamma_m$, so that $n(\tilde{\omega})=\varepsilon(\tilde{\omega})=\mu(\tilde{\omega})$. These conditions can easily be relaxed in favor of a more general approach. The functions under consideration thus provide $n(\tilde{\omega})<0$ for $\tilde{\omega}<1$, and $n(\tilde{\omega})>0$ for $\tilde{\omega}>1$, as shown in Fig. 1. For additional details about the NIM model, the reader is referred to Agranovich *et al.* [55], Shadrivov *et al.* [56], and Popov *et al.* [57], who have analyzed second harmonic generation at an interface between a positive index material and a nonlinear, lossless NIM.

We now consider a variety of conditions that are designed to mimic just as many situations. In all cases we tune the FF pulse and the generated SH signal under phase mismatched conditions. The losses in the Drude model were taken to yield an absorption length larger than 1 mm, and for our purposes losses may be neglected. The pulse then crosses an interface that separates the medium from vacuum, and propagates inside the material. The overall conversion efficiency of the process is low, and so we focus our attention on the dynamics of the interacting pulses. In the first situation,

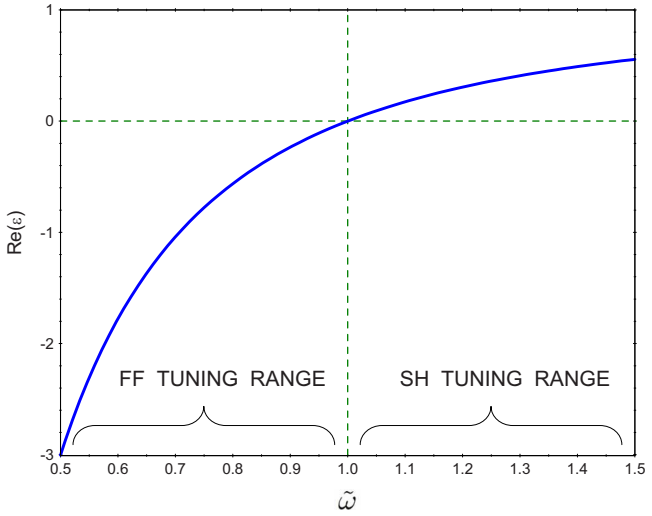

FIG. 1. (Color online) Real part of ε, μ, and n for the Drude model with $\omega_{pe}=\omega_{pm}$. The tuning zones for the FF and the SH are also indicated.

shown in Fig. 2, we consider a super-Gaussian pulse having a spatial extension of approximately 50 microns, incident from vacuum on a dispersive PIM. In the figure we are able to clearly discern the typical spatial modulation that characterizes the generated SH intensity due to the finite coherence length, as the pulse samples the material. The coherence length can be identified as the separation distance between two adjacent peaks in the spatial interference pattern of the SH field intensity. For this reason it is usually defined as the length of material that maximizes SHG, i.e., $L_{\mathrm{coh}}\sim\lambda/2\delta n$. In this particular example, the medium is described by the indices of refraction $n(2\tilde{\omega})=2$ and $n(\tilde{\omega})=1.8$, so that for a generated SH tuned at $\tilde{\omega}=0.7$ the estimated coherence length

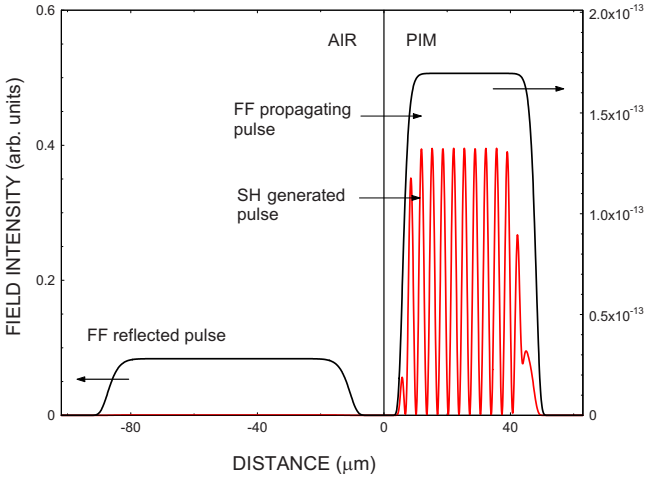

FIG. 2. (Color online) A super-Gaussian pump pulse—scale on left axis—propagates into a positive index material having $n(\tilde{\omega})=1.8$ and $n(2\tilde{\omega})=2.0$ at the fundamental scaled frequency $\tilde{\omega}=0.7$. The assumed dispersion yields group velocities $V_g^{\omega}=c/3.27$ and $V_g^{2\omega}=c/4.08$. Part of the pulse is reflected at the interface, while most of the SH signal is generated forward. We assume $\chi^{(2)}\sim 3\times10^{-7}$ cm/statvolts, or ~ 1 pm/V.

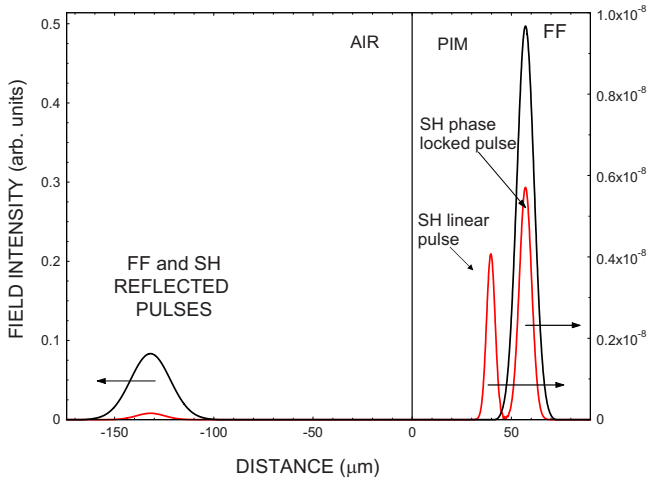

FIG. 3. (Color online) A Gaussian pump pulse—scale on left axis—propagates into a positive index material having $n(\tilde{\omega})=1.47$ and $n(2\tilde{\omega})=1.64$ at the fundamental frequency $\tilde{\omega}=0.84$. The second harmonic signal—scale on right axis—is characterized by a reflected pulse, and two forward-propagating pulses, one traveling at the normal group velocity, which walks off and lags behind, the other phase-locked, and located under the pump and traveling at the pump's group velocity. Here too $\chi^{(2)}\sim 1$ pm/V, and absorption is negligible.

is of order $L_{\mathrm{coh}}\sim 1.75$ μm. From Fig. 2, the calculated spatial modulation of the SH pulse indeed suggests a coherence length $L_{\mathrm{coh}}\sim 1.75$ μm. Because the FF and SH pulses do not propagate far into the medium, the two pulses do not have enough time to experience walkoff.

A more interesting case develops when a short Gaussian pulse is incident on the medium, and the resulting pulses are allowed to propagate in a way that the GVM causes pulse walkoff effects. This case is depicted in Fig. 3 for a pulse tuned at $\tilde{\omega}=0.84$. The incident electric field pulse is approximately 15 wave cycles in duration [full width at half maximum (FWHM)], with peak intensity of 1 W/cm^2. The figure shows that for sufficient propagation distances, one can clearly identify several components: (i) Reflected pump and SH pulses, (ii) a SH pulse that remains and propagates under the pump, and (iii) a normal SH pulse that lags behind, that walks off and propagates with the group velocity associated with the SH frequency. In this situation, the FF pulse appears to capture portion of the generated SH pulse. An almost identical situation develops in a nonlinear $\chi^{(3)}$ medium for third harmonic generation [33].

In trying to assess the intricacies of the dynamics, one may look at the spectra of all propagating components. The frequency spectrum shown in Fig. 4 is obtained by simply monitoring the fields at some spatial location inside the medium as a function of time, and by performing a Fourier transform of that signal. Aside from an evident and inevitable degree of cross-phase modulation experienced by the SH signal, the frequency spectrum does not yield any additional information. The spectrum of the generated SH pulse is compared to the spectrum of a seed SH pulse having similar duration. On the other hand, an analysis of the k-space power spectrum immediately yields valuable information. In

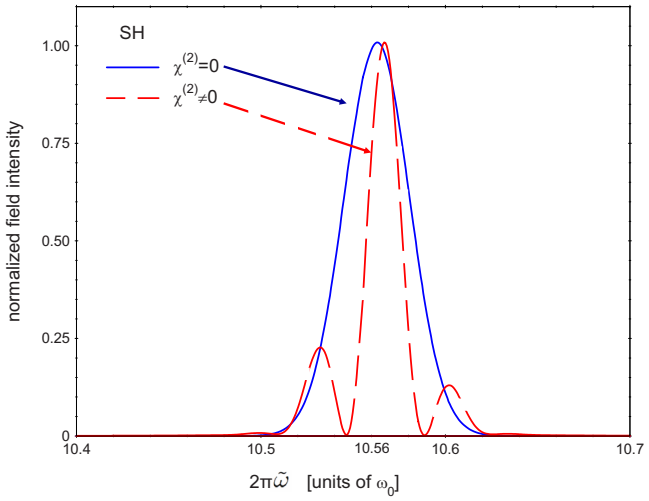

FIG. 4. (Color online) Power spectrum of a generated, forward propagating SH pulse in the presence of a second order nonlinearity (red curve), near the second harmonic frequency $2\tilde{\omega}=1.68$, assuming $n(\tilde{\omega})=1.47$ and $n(2\tilde{\omega})=1.64$. The blue curve is the spectrum of a seed pulse tuned at the second harmonic frequency, having similar duration as the generated SH pulse. The figure shows that the second harmonic pulse undergoes some degree of cross-phase modulation.

Fig. 5 we depict the power spectra of the fields, and analyze all the components for the snapshot corresponding to Fig. 3. For the FF pulse (black curve), we identify the reflected $(-k_\omega)$, and the forward propagating $(k_\omega n_\omega)$ pulses. For the SH signal (red curve), we have (i) a small, backward-generated component $(-k_{2\omega})$, (ii) the normal, forward-moving component that walks off $(k_{2\omega}n_{2\omega})$, and (iii) a phase-

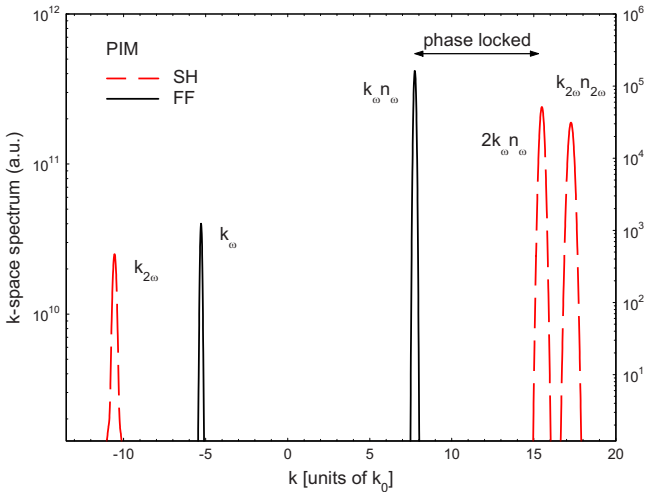

FIG. 5. (Color online) *K*-space power spectrum for the situation depicted Fig. 3. For the pump (FF)—left axis scale—we identify (i) the reflected component $(k_\omega=2\pi\tilde{\omega})$ and (ii) the component that propagates inside the medium $(k_\omega n_\omega)$. For the second harmonic (SH)—right axis scale—it is possible to recognize (i) the reflected component $(k_{2\omega})$, (ii) the component propagating inside the medium that walks off, having nominal group velocity given by material dispersion $(k_{2\omega}n_{2\omega})$, and (iii) the phase-locked component $(2k_\omega n_\omega)$.

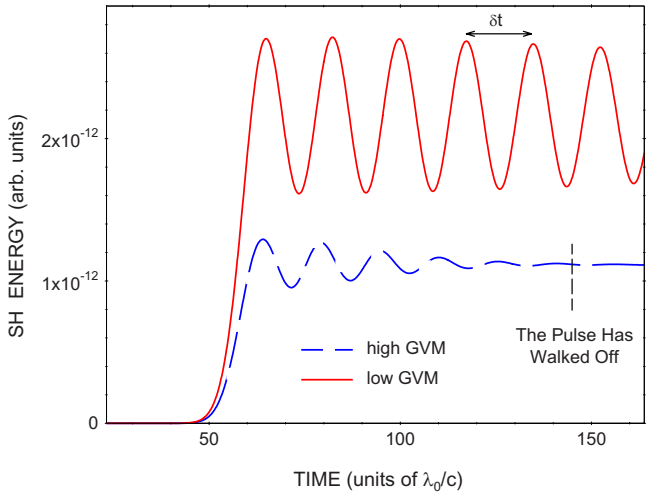

FIG. 6. (Color online) Comparison of energy vs time diagram for SHG under phase mismatched conditions, as follows: (i) Blue curve, large group velocity mismatch (GVM), and (ii) red curve, low GVM. In the first situation, pump duration (FWHM) is approximately 15 reference optical cycles and is tuned to $\tilde{\omega}=0.6$, with $n(\tilde{\omega})=1.41$ and $V_g^\omega=c/2.5$. For the SH we have $n(2\tilde{\omega})=1.52$ and $V_g^{2\omega}=c/4.1$. In the second case, the FF has the same duration, tuning, and index of refraction, but $V_g^\omega=c/2.0$. For the SH $n(2\tilde{\omega})=1.48$ and $V_g^{2\omega}=c/2.2$.

matched component $(2k_\omega n_\omega)$ that corresponds to the SH pulse trapped under the pump. This pulse has a k-vector that satisfies the phase matching condition: $\Delta k=k_{2\omega}n_{2\omega}-2k_\omega n_\omega=0$, and is consistent with the predictions made in references [4] for the quasimonochromatic case.

Ordinarily, the existence of a phase matched component leads to efficient energy conversion. We show the SH energy (Fig. 6) as a function of time for two phase-mismatched situations: (i) A case corresponding to the pulse depicted in Fig. 2, where pulse walkoff has not yet occurred (blue curve), and (ii) the red curve, which describes the situation depicted in Fig. 3, and is indicative of the energy clamping process. Once the normal SH pulse separates, the SH energy quickly settles to a constant, steady state value: The phase matched components is actually phase-locked, a condition that prevents energy exchange to occur. The phase-locking condition is verified by monitoring the phase of the SH pulse as a function of time, at different longitudinal positions. This is a robust phenomenon that does not depend on any threshold intensity or a particular phase mismatch, and the outcome is also stable against the presence of absorption, which generally diminishes total propagation distances, and the kind of nonlinearity [33]. In fact, using our model we report confirmation of the process for the case of a third order nonlinearity and third harmonic generation reported in reference [33]. The energy exchange diagram shown in Fig. 6 suggests that the interaction evolves into a relatively simple phase link between the FF and the SH trapped pulse. It is apparent that the resulting dynamics comes about as a result of a relationship between the phases of the pulses, and not as a material feature. The study of this effect in NIMs will shed more light on the subject, and so we proceed with that in the next section.

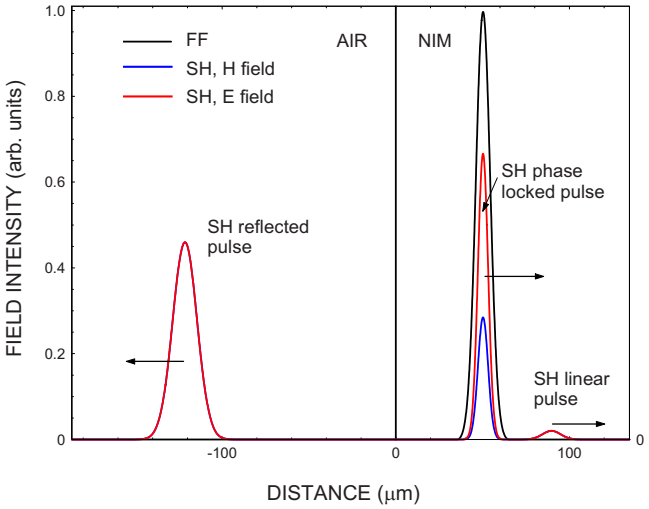

FIG. 7. (Color online) A Gaussian pump pulse—black curve, left axis scale—is tuned to $\tilde{\omega}=0.84$, and propagates into a negative index material such that $n(\tilde{\omega})=-0.41$ and $n(2\tilde{\omega})=0.64$. The second harmonic—red curve, left axis scale—has a reflected pulse, a forward-propagating pulse that leads the way, and propagates at the nominal group velocity for the second harmonic frequency, and a phase-locked pulse that propagates at the group velocity of the fundamental pump field. $\chi^{(2)}=1$ pm/V, and absorption is negligible.

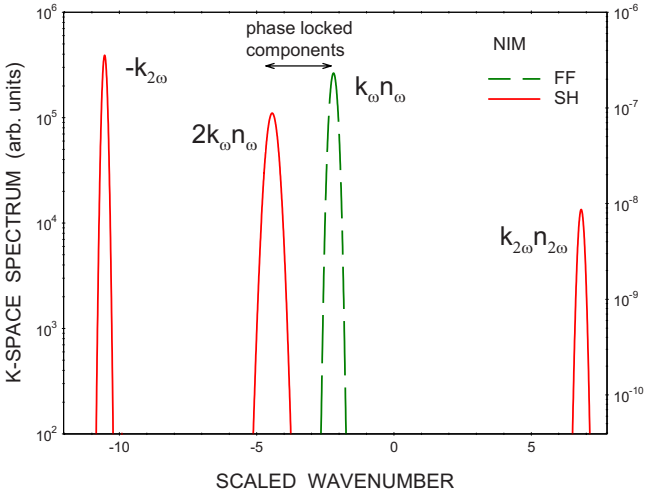

FIG. 8. (Color online) K-space power spectrum of the situation in Fig. 7. For the pump field—left axis scale—we have a forward-propagating component characterized by a negative carrier wave vector ($k_\omega n_\omega$). Pump reflections are negligible. For the second-harmonic wavelength—right axis scale—we identify (i) the reflected component ($-k_{2\omega}$), (ii) the normal component that walks off ($k_{2\omega}n_{2\omega}$), and (iii) the phase-locked component ($2k_\omega n_\omega$). We note that the phase locking condition, $2k_\omega n_\omega = k_{2\omega} n_{2\omega}$, is in general to be distinguished from the material phase matching conditions, $2k_\omega n_\omega = k_{2\omega} n_{2\omega}$.

PULSED SECOND HARMONIC GENERATION IN NEGATIVE INDEX MEDIA

For a case-study of pulsed, phase-matched SHG in NIMs the reader is referred to Ref. [39]. Here we discuss the general case where $\Delta k \neq 0$, and view the phase-matched case as a special case. In Fig. 7 we show the E and H fields for a generic snapshot after the FF crosses the air-NIM interface such that the indices are given by $n(\tilde{\omega})=-0.41$ and $n(2\tilde{\omega})=0.64$ at the FF $\tilde{\omega}=0.84$. The condition $\varepsilon=\mu$ generally yields almost no reflections for the FF, but it allows both forward and backward pulsed SHG [39]. The figure shows that unlike the pump, the E and H fields of the SH pulse separate inside the medium. Typically, this is an indication that the effective parameters ε and μ are no longer the same, just as it occurs in ordinary PIMs. We note that in this case the normal SH pulse that walks off enjoys a larger linear group velocity due to the nature of the Drude dispersion, and so it leads the way.

In Fig. 8 we show the k-spectrum that corresponds to the fields depicted in Fig. 7. Our model sets a negative index of refraction for a normalized frequency $\tilde{\omega}<1$, so if the pump is tuned in the range $0.5<\tilde{\omega}<1$, then the SH always reads a positive index (see captions of Fig. 1, 7, and 8 for details). In Fig. 8 we recognize the following SH components: (i) A reflected SH pulse with k-vector-$k_{2\omega}$; this is the pulse that is generated at the interface and propagates backward in free space; (ii) a forward-propagating pulse with k-vector $k_{2\omega}n_{2\omega}$; this is the normal SH pulse that walks off and leads all pulses; (iii) a phase-locked pulse having k-vector $2k_\omega n_\omega$. The black curve centered at $k_\omega n_\omega$ represents the k-space wave packet of the forward-moving FF pulse. All three SH pulses are generated at the interface, as revealed in Fig. 9, where we monitor the total SH energy as a function of time. All components except the phase-locked pulse are found at the expected spectral positions. Two points are worthy of note: (i) The SH phase-locked pulse is now characterized by a negative wave vector at twice the pump wave vector; (ii) this pulse moves forward at the pump's group velocity. Imprinting the phase-locked pulse with a negative index of refraction results in local separation of the E and H fields, and is the adjustment needed in order to overcome the true dispersive properties of the medium at the SH frequency. In addi-

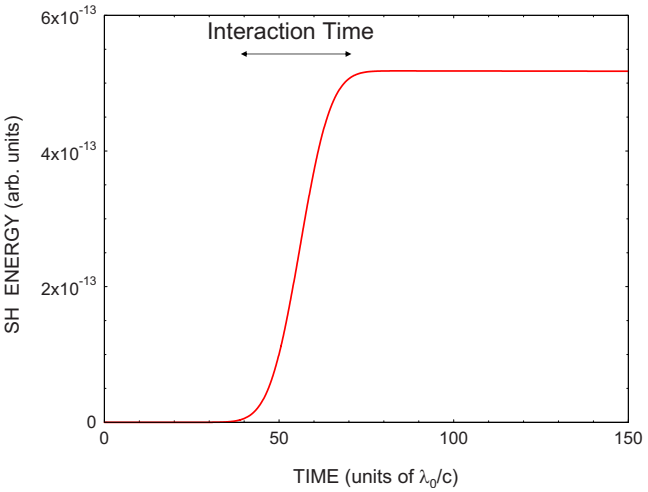

FIG. 9. (Color online) Energy exchange diagram for the situation depicted in Fig. 6. The interaction occurs only during the time under the arrow, which is the time it takes the pulse to cross the interface.

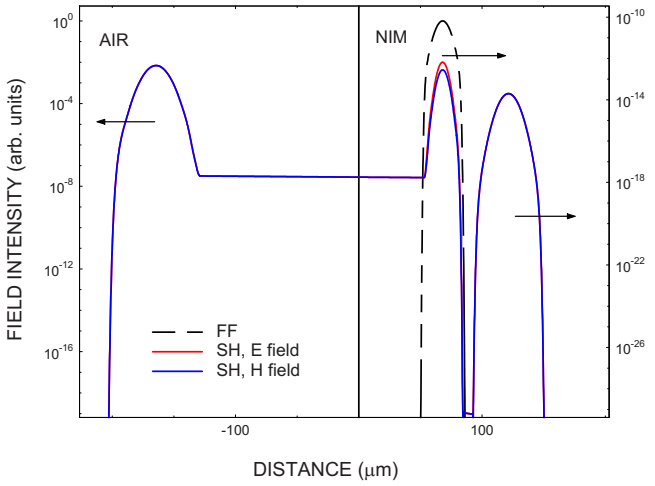

FIG. 10. (Color online) Same situation as in Fig. 6, except that we are now using a semilogarithmic scale. The diagram spans 16 orders of magnitude to show a relative intensity that fills the void between the phase-locked pulse and the backward propagating pulse.

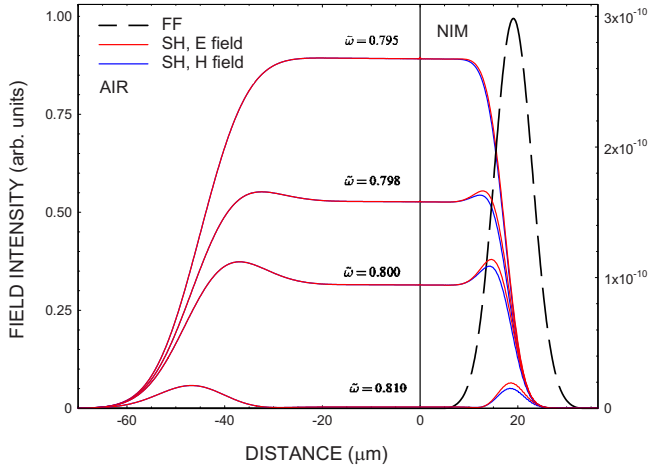

FIG. 11. (Color online) FF pulse—black curve, left axis scale—and SH pulse—red curve, right axis scale—under four different frequency tunings, near and at the phase matching condition at $\tilde{\omega}=0.7905$. The closer one tunes to the phase matching condition, the more the E and H fields overlap, and the more obvious the connection between the phase-locked and the reflected pulse becomes.

tion to causing no reflections, the condition $\varepsilon=\mu$ is necessary for the E and H fields to overlap. Therefore, from Fig. 7 one may appreciate the fact that the E and H fields separate as a result of the phase-locking phenomenon. This separation does not occur for the leading, normal pulse, which still propagates in a NIM with complete E and H overlap.

The dynamics that we have described generally occur only near the interface. Energy exchange stops quickly, without obvious manifestations of spatial modulation of the SH signal, as in Fig. 2. In Fig. 9 we show the SH energy as a function of time, as the pump crosses the interface corresponding to the situation depicted in Fig. 7. The result is a lack of relaxation oscillations, and almost immediate energy clamping. The arrow indicates the duration of the interaction, or the time it takes the pulse to traverse the entry surface.

We also performed simulations where $\omega_{pe}\neq\omega_{pm}$. In this case there exists a range of frequencies where ε and μ have opposite sign, and a gap forms [47]. However, since the FF and the SH frequencies are both tuned out of the gap, there are no qualitative differences between this case and the case presently under consideration, namely $\omega_{pe}=\omega_{pm}$. Additional studies will further clarify both SH and TH behavior when the fields are tuned near the gap or at a transmission resonance.

TWIN PULSES

In Fig. 10 we offer another rendition of Fig. 7, and show the fields on a logarithmic scale that spans sixteen orders of magnitude. The figure suggests a relationship between the backward-propagating packet, and the forward-moving, phase-locked pulse. A more detailed analysis, aided by a parallel development of the FDTD method outlined in Eqs. (3), shows that the phase-locked pulse is releasing light very slowly in the backward direction, an action that creates an umbilical cord and fills the void between the two pulses. We note no such link between the phase-locked pulse and the normal forward-propagating SH component. To further emphasize this link, in Fig. 11 we show SHG corresponding to four tuning conditions at and near the phase matching condition, $\tilde{\omega}_{\mathrm{PM}}=0.7905$. The figure suggests that when the phase matching condition is satisfied, phase-locking and phase-matching become indistinguishable, and the index of refraction of the phase-locked SH signal approaches and matches the material value. Evidence for this is provided by the fact that the degree of E and H field overlap increases as the material phase matching condition nears. Furthermore, the link between the pulses is now more evident, as it is clear that we are dealing with a single, broad, backward-propagating pulse, continuously generated under the envelope of a forward-moving pump, as reported in Ref. [39]. A similar effect occurs in ordinary PIMs, except that phase matching is established in the forward direction, with similar pulse broadening characteristics [29]. Thus one may view the phase matching condition as a special case of the more general features that relate the two pulses, which we refer to as twin pulses. This choice of words will be further clarified in the next section. *The relation* $\Delta k=k_{2\omega}-2k_{\omega}=0$ *is thus established by a portion of the generated SH pulse every time the pump enters the medium, but energy exchange occurs only if the material has the right features to also satisfy it*. This is clear from Fig. 12 where we depict the energy as a function of time for the conditions reported in Fig. 11, as the phase matching conditions are approached.

DISCONTINUITIES

We now examine further twin-pulse generation by introducing a small physical discontinuity inside the NIM, and that is a simple $\chi^{(2)}$ jump (Fig. 13). Although this kind of discontinuity may be considered small by any measure (we

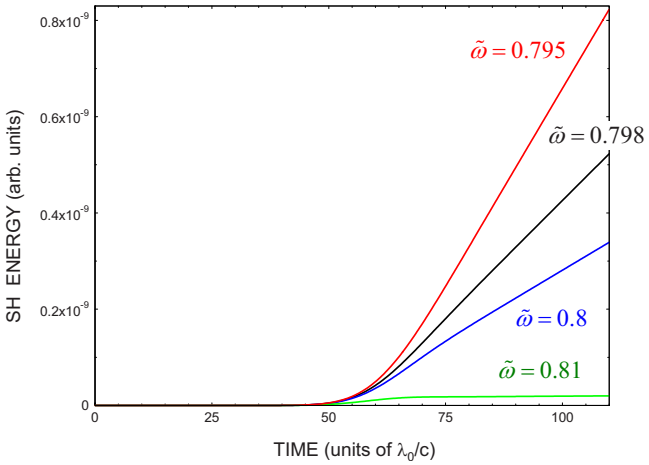

FIG. 12. (Color online) Energy exchange diagram for the situation depicted in Fig. 11.

choose $\chi^{(2)} \sim 1$ pm/V, but the situation persists for arbitrarily small discontinuities), it does nevertheless provide for a break in the translational symmetry of the system. Figures 13–15 form a before, during, and after sequence that sees the FF and SH pulses interact with the above-mentioned discontinuity. While the figures show that the pump continues on unaffected, the SH is almost completely reflected. In fact, crossing the interface generates a small, normal, forward-moving SH pulse, which represents new energy (see Fig. 16). Although we have chosen a small discontinuity to highlight the degree of stability of the phenomenon, a more substantial discontinuity, such as returning the pulse into vacuum also leads to a similar result. Therefore, any discontinuity appears to be enough to set the phase-locked pulse free from the FF pulse, and to send it propagating backward (Fig. 15). Following disengagement, the absence of a link with the pump returns the phase-locked pulse to a normal, backward-

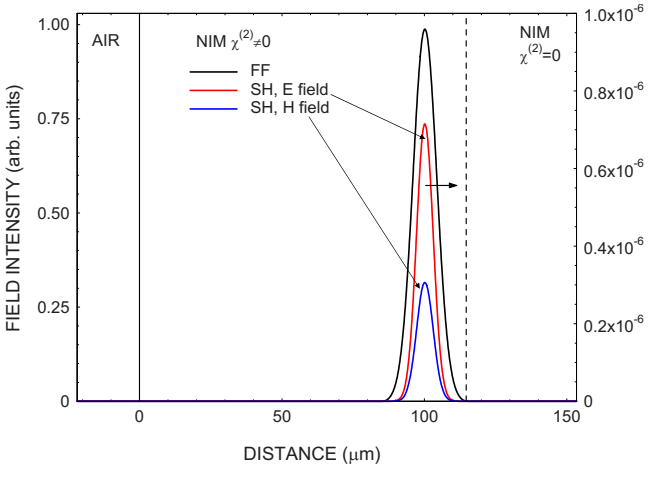

FIG. 13. (Color online) A Gaussian pulse tuned to $\tilde{\omega}=0.84$—black curve, left axis scale—propagates into a negative index material having $n(\tilde{\omega})=-0.41 n(\tilde{\omega})=-0.41$ and $n(2\tilde{\omega})=0.64$, just before a $\chi^{(2)}$ interface is crossed. The phase-locked SH pulse—red and blue curves, right axis scale—propagates at the same group velocity as the FF. $\chi^{(2)}=1$ pm/V, and absorption is negligible.

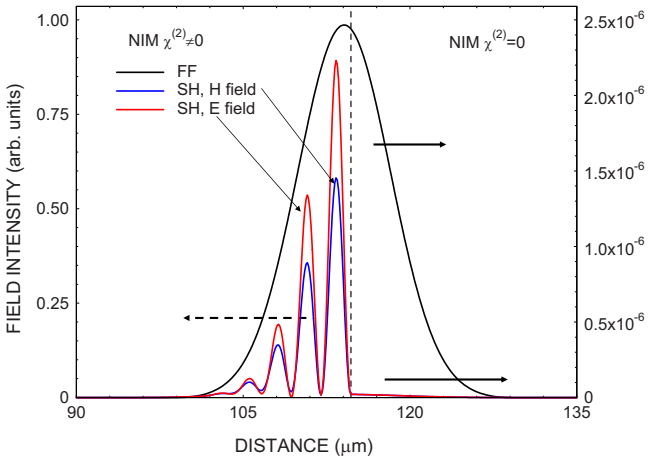

FIG. 14. (Color online) The same pulses of Fig. 13 during the $\chi^{(2)}$ interface crossing. Note that the FF pulse crosses undisturbed, while the SH pulse is stopped as a second forward-moving SH pulse begins to form to the right of the interface.

propagating trajectory: The E and H fields again overlap, with matching spectral components (k-space) at their expected positions. Figure 16 shows that the interface crossing causes the SH signal to gain a small amount of energy. We can reasonably suppose that this energy arises only from the new small, forward-propagating pulse pictured in Fig. 15, and that the phase-locked pulse is simply released without any further energy exchange.

We find that the process will repeat if we reestablish the condition of $\chi^{(2)}>0$ at a position downrange. That is, a new phase-locked pulse is generated as the pump enters the region, and the process begins again. This dynamics suggests that we may set up a NIM-grating such that the $\chi^{(2)}$ alternates between a maximum and a minimum value (Fig. 17). The calculations then suggest that continuous SH generation is also possible, as depicted in Fig. 17 (inset). As the pump pulse traverses the grating, phase-locked subpulses are gen-

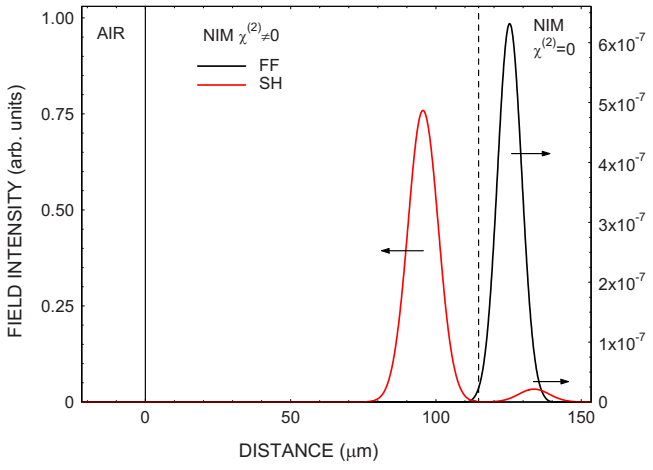

FIG. 15. (Color online) The same pulses of Fig. 13 after the $\chi^{(2)}$ interface crossing. The phase-locked pulse is now freely propagating backward with the group velocity dictated by material dispersion, and a forward-propagating SH pulse is also clearly visible.

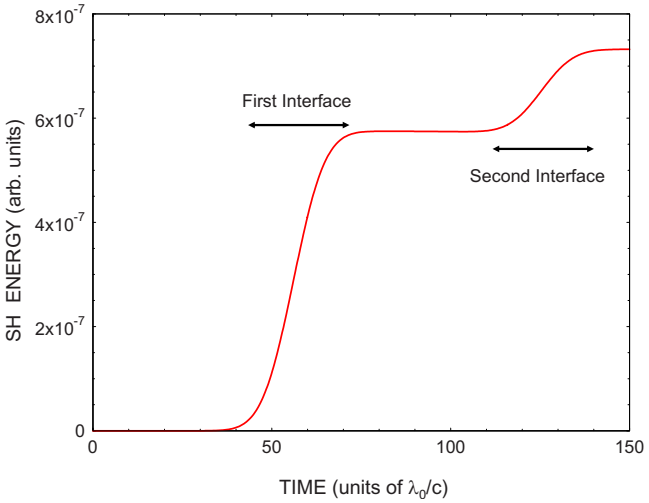

FIG. 16. (Color online) Energy exchange diagram for the situations depicted in Figs. 13–15. SH gain occurs every time a $\chi^{(2)}$ interface is crossed, while between interfaces the energy of the SH pulse clamps.

erated and are repeatedly sent propagating backwards in regular fashion. Another interesting question relates to the grating pitch. In Fig. 18 we show the SHG efficiency vs. the period of the grating for three different situations: (i) $[2\chi^{(2)}|null]$; (ii) $[\chi^{(2)}|-\chi^{(2)}]$; (iii) $[\chi^{(2)}|null]$. By *null* here we mean a zero $\chi^{(2)}$ coefficient. Although the behavior is similar in all three cases, it is also evident that optimal conditions for SHG may be sought and found.

SEMIANALYTICAL TREATMENT

It is possible to draw some conclusions about the phase-locking mechanism based on the semianalytical treatment

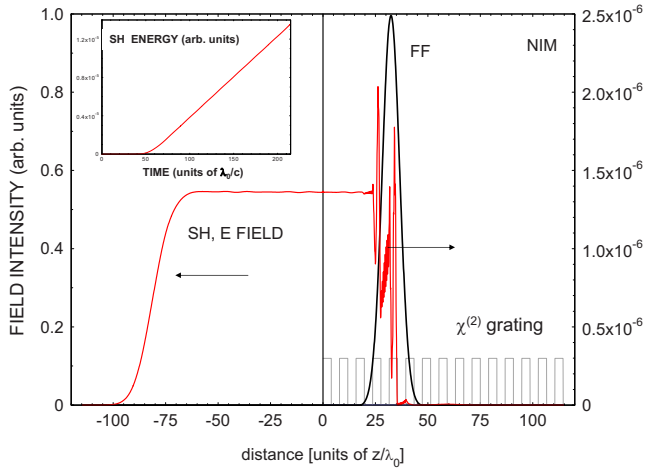

FIG. 17. (Color online) A Gaussian pump pulse propagates inside a NIM having a grating of $\chi^{(2)}$ having a period of eight reference wavelengths, and alternating between values of zero and $\chi^{(2)}=1$ pm/V. $n(\tilde{\omega})=-0.41$ and $n(2\tilde{\omega})=0.64$ at the FF tuning of $\tilde{\omega}=0.84$. Inset: SH energy vs time as the pump pulse plows through the grating.

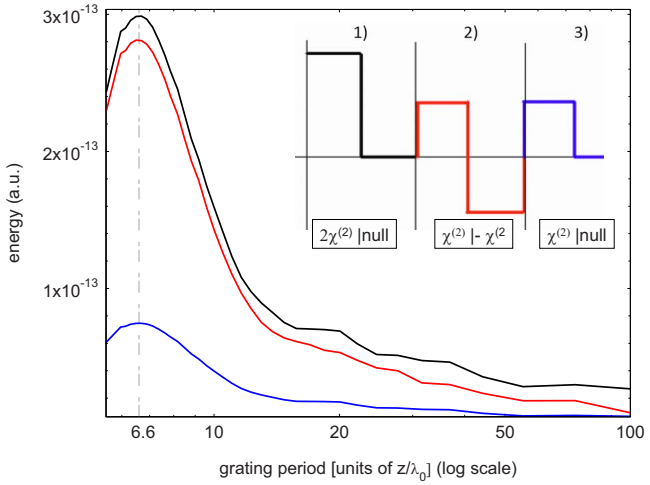

FIG. 18. (Color online) SH energy as a function of grating period for three different situations. Note that in all cases the maximum gain occurs for the same grating period, namely ~6.6 reference wavelengths.

described in reference [33]. Since we are dealing with NIMs, we use a set of coupled nonlinear generalized Schrödinger equations to describe the interaction between the FF and SH pulses [58]. We write

$$\frac{\partial E_\omega}{\partial z} = \frac{ik_\omega''}{2}\frac{\partial^2 E_\omega}{\partial t^2} + \frac{i\beta\mu_\omega\chi^{(2)}}{2n_\omega}E_\omega^* E_{2\omega},$$

$$\frac{\partial E_{2\omega}}{\partial z} = \frac{ik_{2\omega}''}{2}\frac{\partial^2 E_{2\omega}}{\partial t^2} + \frac{i\beta\mu_{2\omega}\chi^{(2)}}{n_{2\omega}}E_\omega^2, \tag{6}$$

where $k''=\partial(1/V_g)/\partial\omega$ is the group velocity dispersion coefficient, and z and t represent retarded coordinates that ride with the wave. As written, Eqs. (6) select the phase locked FF and SH components that co-propagate at the same group velocity, and neglects the SH pulse that walks off. The conditions that are satisfied in the regime that we consider, a pump field much more intense than the SH field, dictate the pump amplitude be constant along z. We may further write the complex field envelope functions in terms of phase and amplitude as follows:

$$E_{\omega,2\omega} = A_{\omega,2\omega}\exp(i\phi_{\omega,2\omega}), \tag{7}$$

and expand the second of Eqs. (6), so that we have

$$\frac{\partial A_{2\omega}}{\partial z} = -k''\frac{\partial A_{2\omega}}{\partial t}\frac{\partial \phi_{2\omega}}{\partial t} - \frac{k''}{2}A_{2\omega}\frac{\partial^2\phi_{2\omega}}{\partial t^2} - \beta\frac{\chi^{(2)}}{2}\sqrt{\frac{\mu}{\varepsilon}}A_\omega^2\sin(2\phi_\omega - \phi_{2\omega}), \tag{8a}$$

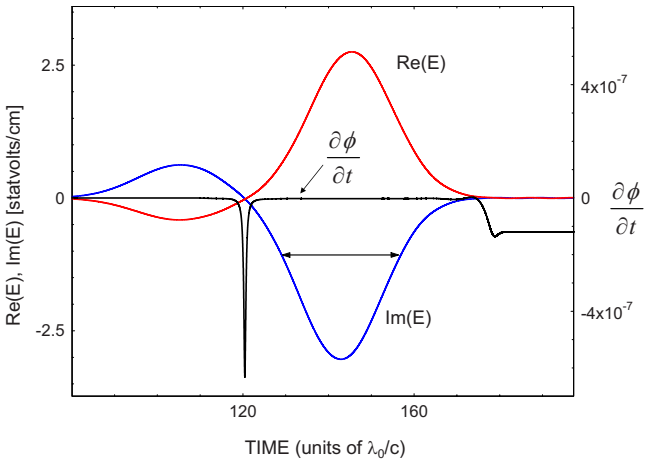

FIG. 19. (Color online) Time derivative of the phase (black curve, right axis) at the observation point located at $\xi \sim 36$ (microns), and the real (blue curve, left axis) and imaginary (red curve, left axis) parts of the field at the same location.

$$\frac{A_{2\omega}}{A_\omega^2}\frac{\partial\phi_{2\omega}}{\partial z} = \frac{k''}{2A_\omega^2}\frac{\partial^2 A_{2\omega}}{\partial t^2} - k''\frac{A_{2\omega}}{2A_\omega^2}\left(\frac{\partial\phi_{2\omega}}{\partial t}\right)^2 + \beta\frac{\chi^{(2)}}{2}\sqrt{\frac{\mu}{\varepsilon}}\cos(2\phi_\omega - \phi_{2\omega}). \quad (8b)$$

In the retarded coordinate, we put $\partial A_{2\omega}/\partial z \simeq \partial\phi_{2\omega}/\partial z \simeq 0$. It is possible to estimate numerically the temporal derivative of the phase at any longitudinal position, and we find that $\partial\phi_{2\omega}/\partial t = \text{const} \ll 1[1/s']$, where $s' = \lambda_0/c$ is the normalized time of magnitude 10^{-14} s. It follows that $\partial^2\phi_{2\omega}/\partial t^2 = 0$. In Fig. 19 we show typical field profiles as functions of time at an observation point inside the medium, obtained by integrating Eqs. (3). In the figure, the right axis depicts the derivative of the phase, and it is evident that inside the pulse (the region illustrated by the arrow) it is indeed a very small constant number. Similar results are obtained at different observation points. We may also estimate $\partial^2 A_{2\omega}/\partial t^2 \simeq 0$ numerically using similar arguments. We also find that the term $k''(\partial A_{2\omega}/\partial t)(\partial\phi_{2\omega}/\partial t)$ is nearly three orders of magnitude smaller than the last term in Eq. (8a). The equations then reduce to

$$\beta\frac{\chi^{(2)}}{2}\sqrt{\frac{\mu}{\varepsilon}}A_\omega^2\sin(2\phi_\omega - \phi_{2\omega}) \approx 0, \quad (9a)$$

$$\cos(2\phi_\omega - \phi_{2\omega}) \approx \frac{k''}{\beta\chi^{(2)}}\frac{A_{2\omega}}{A_\omega^2}\left(\frac{\partial\phi_{2\omega}}{\partial t}\right)^2\sqrt{\frac{\varepsilon}{\mu}}. \quad (9b)$$

Equation (9a) allows the nontrivial solution only if $2\phi_\omega - \phi_{2\omega} = 0$. This is the phase-locked condition for the SH pulse. This is consistent with Eq. (9b), because we are also able to verify that $(\partial\phi_{2\omega}/\partial t)^2\sqrt{\varepsilon/\mu}(k''A_{2\omega}/\beta\chi^{(2)}A_\omega^2) \simeq 1$, so that $\cos(2\phi_\omega - \phi_{2\omega}) \simeq 1$.

To conclude this section, we observe that the conditions we have applied in the low intensity regime, namely that the pump ad SH are constants in z, are similar to conditions that one usually applies to seek soliton solutions. In negative index media, for example, simultons have been reported in nonlinearly quadratic media, in a high intensity, strong coupling regime [59]. Simultons are two-frequency waves that copropagate in a given direction, that nevertheless resemble the pump-SH pair of pulses that we have described above. On the other hand, at low intensities solitons may not form, and the two-color components may propagate in opposite directions. Therefore, connections and similarities between the basic phase-locking mechanism that we report here and the phase-locking reported in the case of multicolor solitons [5,59] in the high intensity regime are inescapable, and may indeed provide the basis for further understanding these processes.

CONCLUSIONS

We have analyzed pulsed SHG in ordinary and negative index materials under phase mismatched conditions, and find that a portion of the generated second-harmonic signal is phase locked, trapped and dragged along by the pump pulse. In the case of negative index materials, it turns out that the trapped pulse and the pulse back-reflected at the interface constitute a set of twin pulses having the same negative wave vector but propagating in opposite directions as a result of the trapping mechanism. Our work thus extends previous investigations done in ordinary materials, and bridges the gap with metamaterials by revealing exciting new dynamical characteristics hitherto unknown. The experimental realization of this phenomenon requires a relatively low loss negative index material in the infrared and optical frequency regime. While such materials are not readily available yet, recent developments in the fabrication of a negative index metamaterial in the infrared regime are already encouraging.

These results thus constitute a first step toward better understanding of the dynamics of ultrashort pulse propagation phenomena under phase mismatched conditions, followed by a natural extension of our model to two dimensions. The inclusion of transverse effects and the consideration of simultaneous, competing second and third order nonlinearities thus constitute fertile ground for continued research.

[1] P. A. Franken, A. E. Hill, C. W. Peters, and G. Weinreich, Phys. Rev. Lett. **7**, 118 (1961).
[2] J. A. Giordmaine, Phys. Rev. Lett. **8**, 19 (1962).
[3] P. D. Maker, R. W. Terhune, M. Nisenoff, and C. M. Savage, Phys. Rev. Lett. **8**, 21 (1962).
[4] J. A. Armstrong, N. Bloembergen, J. Ducuing, and P. S. Pershan, Phys. Rev. **127**, 1918 (1962); N. Bloembergen and P. S. Pershan, *ibid.* **128**, 606 (1962).
[5] K. Beckwitt, Y. F. Chen, F. W. Wise, and B. A. Malomed, Phys. Rev. E **68**, 057601 (2003).
[6] M. M. Fejer, G. A. Magel, D. H. Jundt, and R. L. Byer, IEEE J. Quantum Electron. **28**, 2631 (1992).
[7] U. Sapaev and D. Reid, Opt. Express **13**, 3264 (2005).
[8] G. D. Boyd and C. K. N. Patel, Appl. Phys. Lett. **8**, 12 (1966).
[9] E. V. Petrov and B. I. Mantsyzov, JETP **101**, 3 (2005).
[10] M. G. Weber, Phys. Rev. B **33**, 6775 (1986).
[11] E. Sidick, A. Knoesen, and A. Dienes, Pure Appl. Opt. **5**, 709 (1996).
[12] D. T. Reid, J. Opt. A, Pure Appl. Opt. **5**, S97 (2003).
[13] A. Steinbach, M. Rauner, F. C. Cruz, and J. C. Bergquist, Opt. Commun. **123**, 207 (1996).
[14] G. D'Aguanno, N. Mattiucci, M. J. Bloemer, and M. Scalora, Phys. Rev. E **74**, 036605 (2006).
[15] K. Gallo, P. Baldi, M. De Micheli, D. B. Ostrowsky, and G. Assanto, Opt. Lett. **25**, 13 (2000).
[16] C. Conti, G. Assanto, and S. Trillo, Opt. Lett. **24**, 16 (1999).
[17] N. Fujioka, S. Ashihara, H. Ono, T. Shimura, and K. Kuroda, Opt. Lett. **31**, 18 (2006).
[18] M. Scalora, M. J. Bloemer, A. S. Manka, J. P. Dowling, C. M. Bowden, R. Viswanathan, and J. W. Haus, Phys. Rev. A **56**, 3166 (1997).
[19] M. Centini, G. D'Aguanno, M. Scalora, C. Sibilia, M. Bertolotti, M. J. Bloemer, and C. M. Bowden, Phys. Rev. E **64**, 046606 (2001).
[20] T. Wang, L. Qian, H. Zhu, Z. Hou, and F. Li, Opt. Commun. **188**, 213 (2001).
[21] V. Krylov, A. Rebane, A. G. Kalintsev, H. Schwoerer, and U. P. Wild, Opt. Lett. **20**, 2 (1995).
[22] Y. Liu and J. C. Diels, IEEE J. Quantum Electron. **42**, 8 (2006).
[23] F. Xu, J. L. He, J. Liao, Q. Wang, Q. Xu, N. H. Shen, H. T. Wang, and N. B. Ming, Phys. Rev. A **68**, 053803 (2003).
[24] S. Orlov, A. Yariv, and M. Segev, Appl. Phys. Lett. **68**, 12 (1996).
[25] S. L. Shapiro, Appl. Phys. Lett. **13**, 19 (1968).
[26] W. H. Glenn, IEEE J. Quantum Electron. **QE-5**, 6 (1969).
[27] M. M. Fejer, Phys. Today **47**, 25 (1994).
[28] J. T. Manassah and O. R. Cockings, Opt. Lett. **12**, 12 (1987).
[29] L. D. Noordam, H. J. Bakker, M. P. de Boer, and H. B. van Linden van den Heuvell, Opt. Lett. **15**, 24 (1990).
[30] R. Maleck Rassoul, A. Ivanov, E. Freysz, A. Ducasse, and F. Hache, Opt. Lett. **22**, 268 (1997).
[31] W. Su, L. Qian, H. Luo, X. Fu, H. Zhu, T. Wang, K. Beckwitt, Y. Chen, and F. Wise, J. Opt. Soc. Am. B **23**, 51 (2006).
[32] M. Mlejnek, E. M. Wright, J. V. Moloney, and N. Bloembergen, Phys. Rev. Lett. **83**, 2934 (1999).
[33] N. Aközbek, A. Iwasaki, A. Becker, M. Scalora, S. L. Chin, and C. M. Bowden, Phys. Rev. Lett. **89**, 143901 (2002).
[34] Y. S. Kivshar, Phys. Rev. E **51**, 1613 (1995).
[35] C. Conti, S. Trillo, and G. Assanto, Phys. Rev. Lett. **92**, 120404 (1997).
[36] C. Conti, S. Trillo, and G. Assanto, Opt. Lett. **23**, 5 (1998).
[37] C. Conti, S. Trillo, and G. Assanto, Opt. Lett. **22**, 17 (1997).
[38] Llous Torres and E. M. Wright, J. Opt. Soc. Am. B **13**, 864 (1996).
[39] S. A. Ramakrishna, Rep. Prog. Phys. **68**, 449 (2005).
[40] V. G. Veselago, Sov. Phys. Usp. **10**, 509 (1968).
[41] J. B. Pendry, A. J. Holden, D. J. Robbins, and W. J. Stewart, IEEE Trans. Microwave Theory Tech. **47**, 2075 (1999).
[42] D. R. Smith, W. J. Padilla, D. C. Vier, S. C. Nemat-Nasser, and S. Schultz, Phys. Rev. Lett. **84**, 4184 (2000).
[43] G. Dolling, M. Wegener, C. M. Soukoulis, and S. Linden, Opt. Lett. **32**, 53 (2007); U. K. Chettiar, A. V. Kildishev, H.-K. Yuan, W. Cai, S. Xiao, V. P. Drachev, and V. M. Shalaev, *ibid.* **32**, 1671 (2007).
[44] S. Linden, C. Enkrich, M. Wegener, J. Zhou, T. Koschny, and C. M. Soukoulis, Science **306**, 1351 (2004); V. M. Shalaev, W. Cai, U. K. Chettiar, H. Yuan, A. K. Sarychev, V. P. Drachev, and A. V. Kildishev, Opt. Lett. **30**, 3356 (2005).
[45] I. Kourakis and P. K. Shukla,Phys. Rev. E **72**, 016626 (2005).
[46] M. Scalora, G. D'Aguanno, M. Bloemer, M. Centini, D. de Ceglia, N. Mattiucci, and Y. S. Kivshar, Opt. Express **14**, 4746 (2006).
[47] M. Scalora, D. de Ceglia, G. D'Aguanno, N. Mattiucci, N. Akozbek, M. Centini, and M. J. Bloemer, Phys. Rev. E **75**, 066606 (2007).
[48] R. W. Ziolkowski and E. Heyman, Phys. Rev. E **64**, 056625 (2001).
[49] D. de Ceglia, A. D'Orazio, M. De Sario, V. Petruzzelli, F. Prudenzano, M. Centini, M. G. Cappeddu, M. J. Bloemer, and M. Scalora, Opt. Lett. **32**, 3 (2007).
[50] M. D. Feit and J. A. Fleck, Appl. Opt. **17**, 3990 (1978); **19**, 2240 (1980).
[51] M. Scalora and M. E. Crenshaw, Opt. Commun. **108**, 191 (1994); M. Scalora, in *Nanoscale linear and nonlinear optics*, edited by M. Bertolotti, C. M. Bowden, and S. Sibilia. AIP Conf. Proc. No. 560 (AIP, Melville, NY, 2001), p. 298.
[52] M. Scalora, G. D'Aguanno, N. Mattiucci, N. Akozbek, M. J. Bloemer, M. Centini, C. Sibilia, and M. Bertolotti, Phys. Rev. E **72**, 066601 (2005).
[53] M. Scalora, G. D'Aguanno, N. Mattiucci, M. J. Bloemer, J. W. Haus, and A. M. Zheltikov, Appl. Phys. B: Lasers Opt. **81**, 393 (2005).
[54] W. Zheng, W. Han, L. Qian, P. Yuan, G. Xie, H. Luo, H. Zhu, and D. Fan, J. Opt. A, Pure Appl. Opt. **8**, 939 (2006).
[55] V. M. Agranovich, Y. R. Shen, R. H. Baughman, and A. A. Zakhidov, Phys. Rev. B **69**, 165112 (2004).
[56] I. V. Shadrivov, A. A. Zharov, and Y. S. Kivshar, J. Opt. Soc. Am. B **23**, 529 (2006).
[57] A. K. Popov and V. M. Shalaev, Opt. Lett. **31**, 2169 (2006); Appl. Phys. B: Lasers Opt. **84**, 131 (2006); A. K. Popov, V. V. Slabko, and V. M. Shalaev, Laser Phys. Lett. **3**, 293 (2006).
[58] M. Scalora, M. S. Syrchin, N. Akozbek, E. Y. Poliakov, G. D'Aguanno, N. Mattiucci, M. J. Bloemer, and A. M. Zheltikov, Phys. Rev. Lett. **95**, 013902 (2005).
[59] A. I. Maismitov, I. R. Gabitov, and E. V. Kazantseva, Opt. Spectrosc. **102**, 90 (2007).